INSTITUTE OF PHYSICS PUBLISHING CLASSICAL AND QUANTUM GRAVITY

Class. Quantum Grav. **23** (2006) 3763–3782 doi:10.1088/0264-9381/23/11/006

Parameter estimation of compact binaries using the inspiral and ringdown waveforms

Manuel Luna[1] **and Alicia M Sintes**[1,2]

[1] Departament de Física, Universitat de les Illes Balears, Cra. Valldemossa Km 7.5, E-07122 Palma de Mallorca, Spain
[2] Max-Planck-Institut für Gravitationsphysik, Albert Einstein Institut, Am Mühlenberg 1, D-14476 Golm, Germany

E-mail: manuel.luna@uib.es and sintes@aei.mpg.de

Received 18 January 2006
Published 3 May 2006
Online at stacks.iop.org/CQG/23/3763

Abstract

We analyse the problem of parameter estimation for compact binary systems that could be detected by ground-based gravitational wave detectors. So far, this problem has only been dealt with for the inspiral and the ringdown phases separately. In this paper, we combine the information from both signals, and we study the improvement in parameter estimation, at a fixed signal-to-noise ratio, by including the ringdown signal without making any assumption on the merger phase. The study is performed for both initial and advanced LIGO and VIRGO detectors.

PACS numbers: 04.80.Nn, 95.55.Ym, 97.60.Gb, 07.05.Kf

1. Introduction

Coalescing compact binaries consisting of either black holes (BH) or neutron stars (NS) are among the targets of ongoing searches for gravitational waves in the data of ground-based interferometric detectors such as GEO 600 [1, 2], the Laser Interferometer Gravitational Wave Observatory (LIGO) [3, 4], TAMA 300 [5] and VIRGO [6].

The coalescence of a compact binary system is commonly divided into three stages, which are not very well delimited one from another, namely the inspiral, the merger and the ringdown. Many studies so far have focused on the gravitational waves emitted during the inspiral phase because the inspiral waveform is very well understood [7–14] and the event rates seem promising [15–19]. Gravitational waves from the merger can only be calculated using the full Einstein equations. Because of the extreme strong field nature of this epoch, neither a straightforward application of post-Newtonian theory nor perturbation theory is very useful. Recent numerical work [20–24] has given some insights into the merger problem, but there are no reliable models for the waveform of the merger phase at this time. The gravitational

radiation from the ringdown phase is also well known and it can be described by quasi-normal modes [25]. In spite of the importance of the ringdown, there are fewer publications on ringdown searches compared to those for inspiral searches.

Flanagan and Hughes [26] were the first in studying the contribution of the three phases to the signal-to-noise ratios for both ground-based and space-based interferometers, but they did not study the problem of accuracy in the parameter estimation. This is an important problem because many efforts are now underway to detect both the inspiral and the ringdown signals using matched filtering techniques in real data [27–31]. In a recent paper [32], parameter estimation of inspiralling compact binaries has been revised using up to the 3.5 restricted post-Newtonian approximation, extending previous analysis [33, 34], but ignoring the other stages. The parameter estimation for the ringdown phase alone has also been studied, some time ago, for ground-based detectors [35–37] as well as for LISA [38]. The aim of this paper is to discuss how parameter estimation can be improved by using information from both the inspiral and the ringdown phases combined together in matched filtering like analysis for different ground-based detectors.

This paper is organized as follows: section 2 introduces our notation and reviews the basic concepts of signal parameter estimation in matched filtering. Section 3 provides the noise curves used in this study for initial and advanced LIGO and VIRGO. Section 4 briefly describes the waveforms that we are looking for. For the inspiral phase, we consider a non-spinning compact system with circular orbits and the waveform in the restricted post-Newtonian approximation. For the ringdown, we assume that the dominant mode has $l = m = 2$ and therefore the waveform is given by an exponentially decaying sinusoid. Section 5 studies the impact on the parameter estimation for coalescing binary black holes, by combining the signals from both the inspiral and ringdown phases, and compares the results with the case of inspiral phase alone. The results are presented for a fixed inspiral signal-to-noise ratio of 10. Different numbers of parameters are used as well as different values for the ringdown efficiency. Finally, section 6 concludes with a summary of our results and plans for further work. In the appendices, we collect various technical calculations, and we present an explicit analytical calculation of the Fisher matrix for the ringdown phase that has been used to compare with the numerical results.

2. Summary of parameter estimation

In this section, we briefly review the basic concepts and formulae of signal parameter estimation relevant to the goal of this paper; we refer the reader to [33] for a more detailed analysis.

The output of a gravitational wave detector can be schematically represented as

$$s(t) = h(t) + n(t), \tag{1}$$

where $n(t)$ is the noise that affects the observation and $h(t)$ is the gravitational wave signal measured at the detector, a linear superposition of the two independent polarizations of the strain amplitude h_+ and $h_\times$, given by

$$h(t) = F_+(\theta, \phi, \psi)h_+(t) + F_\times(\theta, \phi, \psi)h_\times(t), \tag{2}$$

where F_+ and $F_\times$ are the antenna pattern functions that depend on the direction of the source in the sky (θ, ϕ) and the polarization angle ψ. In the case of a laser interferometer detector, the expressions for F_+ and $F_\times$ are given by [44]

$$F_+(\theta, \phi, \psi) = \tfrac{1}{2}(1 + \cos^2\theta)\cos 2\phi \cos 2\psi - \cos\theta \sin 2\phi \sin 2\psi, \tag{3}$$

$$F_\times(\theta, \phi, \psi) = \tfrac{1}{2}(1 + \cos^2\theta)\cos 2\phi \sin 2\psi + \cos\theta \sin 2\phi \cos 2\psi. \tag{4}$$

For sake of simplicity, we shall make the standard assumptions that the noise $n(t)$ has zero mean and it is stationary and Gaussian, although in realistic cases this hypothesis is likely to be violated at some level. Within this approximation, the Fourier components of the noise are statistically described by

$$E[\tilde{n}(f)\tilde{n}^*(f')] = \tfrac{1}{2}\delta(f - f')S_n(f), \tag{5}$$

where $E[\cdot]$ denotes the expectation value with respect to an ensemble of noise realization, the * superscript denotes complex conjugate, $S_n(f)$ is the one-sided noise power spectral density and tildes denote Fourier transforms according to the convention

$$\tilde{x}(f) = \int_{-\infty}^{\infty} \mathrm{e}^{\mathrm{i}2\pi f t} x(t)\,\mathrm{d}t. \tag{6}$$

With a given noise spectral density for the detector, one defines the 'inner product' between any two signals $g(t)$ and $h(t)$ by

$$(g|h) \equiv 2\int_0^{\infty} \frac{\tilde{g}^*(f)\tilde{h}(f) + \tilde{g}(f)\tilde{h}^*(f)}{S_n(f)}\,\mathrm{d}f. \tag{7}$$

With this definition, the probability of the noise to have a realization n_0 is just

$$p(n = n_0) \propto \mathrm{e}^{(n_0|n_0)/2}. \tag{8}$$

The optimal signal-to-noise ratio (SNR) ρ, achievable with linear methods (e.g., matched filtering the data) is given by the standard expression

$$\rho^2 = (h|h) = 4\int_0^{\infty} \frac{|\tilde{h}(f)|^2}{S_n(f)}\,\mathrm{d}f. \tag{9}$$

In the limit of large SNR, if the noise is stationary and Gaussian, the probability that the gravitational wave signal $h(t)$ is characterized by a given set of values of the source parameters $\boldsymbol{\lambda} = \{\lambda^k\}_k$ is given by a Gaussian probability of the form [35]

$$p(\boldsymbol{\lambda}|h) = p^{(0)}(\boldsymbol{\lambda}) \exp\left[-\tfrac{1}{2}\Gamma_{jk}\Delta\lambda^j\Delta\lambda^k\right], \tag{10}$$

where $\Delta\lambda^k$ is the difference between the true value of the parameter and the best-fit parameter in the presence of some realization of the noise, $p^{(0)}(\boldsymbol{\lambda})$ represents the distribution of prior information (a normalization constant) and Γ_{jk} is the so-called Fisher information matrix defined by

$$\Gamma_{ij} \equiv (\partial_i h|\partial_j h) = 2\int_0^{\infty} \frac{\partial_i\tilde{h}^*(f)\partial_j\tilde{h}(f) + \partial_i\tilde{h}(f)\partial_j\tilde{h}^*(f)}{S_n(f)}\,\mathrm{d}f, \tag{11}$$

where $\partial_i = \frac{\partial}{\partial\lambda^i}$.

The inverse of the Fisher matrix, known as the variance–covariance matrix, gives us the accuracy with which we expect to measure the parameters λ^k

$$\Sigma^{jk} \equiv (\Gamma^{-1})^{jk} = \langle\Delta\lambda^j\Delta\lambda^k\rangle. \tag{12}$$

Here the angle brackets denote an average over the probability distribution function in equation (10). The root-mean-square error σ_k in the estimation of the parameters λ^k can then be calculated, in the limit of large SNR, by taking the square root of the diagonal elements of the variance–covariance matrix,

$$\sigma_k = \langle(\Delta\lambda^k)^2\rangle^{1/2} = \sqrt{\Sigma^{kk}}, \tag{13}$$

and the correlation coefficients c^{jk} between two parameters λ^j and λ^k are given by

$$c^{jk} = \frac{\langle\Delta\lambda^j\Delta\lambda^k\rangle}{\sigma_j\sigma_k} = \frac{\Sigma^{jk}}{\sqrt{\Sigma^{jj}\Sigma^{kk}}}. \tag{14}$$

3. Noise spectra of the interferometers

In this paper, we use three different noise curves to understand the effect of detector characteristics on the parameter estimation. The noise curves used are initial and advanced LIGO and VIRGO as in [32]. These are as follows.

For the initial LIGO,

$$S_n(f) = \begin{cases} S_0[(4.49x)^{-56} + 0.16x^{-4.52} + 0.52 + 0.32x^2], & f \geqslant f_s, \\ \infty, & f < f_s, \end{cases} \tag{15}$$

where $x = f/f_0$, with $f_0 = 150$ Hz (a scaling frequency chosen for convenience), $f_s = 40$ Hz is the lower cut-off frequency and $S_0 = 9 \times 10^{-46}$ Hz^{-1}.

For advanced LIGO, the noise curve is given by

$$S_n(f) = \begin{cases} S_0\left[x^{-4.14} - 5x^{-2} + \frac{111(1-x^2+x^4/2)}{(1+x^2/2)}\right], & f \geqslant f_s, \\ \infty, & f < f_s, \end{cases} \tag{16}$$

where $f_0 = 215$ Hz, $f_s = 10$ Hz and $S_0 = 10^{-49}$ Hz^{-1}.

Finally, for the VIRGO detector, the expected noise curve is given by

$$S_n(f) = \begin{cases} S_0[(6.35x)^{-5} + 2x^{-1} + 1 + x^2], & f \geqslant f_s, \\ \infty, & f < f_s, \end{cases} \tag{17}$$

where $f_0 = 500$ Hz, $f_s = 20$ Hz and $S_0 = 3.24 \times 10^{-46}$ Hz^{-1}.

4. The gravitational wave signal

As discussed in the introduction, the coalescence and its associated gravitational wave signal can be divided into three successive epochs in the time domain: inspiral, merger and ringdown. During the inspiral, the distance between the stars diminishes and the orbital frequency sweeps up. For low-mass binary systems, the waveforms are well modelled using the post-Newtonian approximation to general relativity [7, 9, 10, 13]. Eventually, the post-Newtonian description of the orbit breaks down, and the black holes cannot be treated as point particles any more. What is more, it is expected that they will reach the *innermost stable circular orbit* (ISCO), at which the gradual inspiral ends and the black holes begin to plunge together to form a single black hole. This is referred to as the merger phase. At present, the merger phase is not well understood and no analytical reliable waveforms exist. At the end, the final black hole will gradually settle down into a Kerr black hole. The last gravitational waves will be dominated by the quasi-normal ringing modes of the black hole (see [41] and references therein) and can be treated using perturbation theory [42]. At late time, the radiation will be dominated by the $l = m = 2$ mode [25]. This is the so-called ringdown phase.

The gravitational waveform of coalescing compact binaries thus takes the form

$$h(t) = \begin{cases} h_{\text{inspiral}}(t), & -\infty < t < T_{\text{ISCO}}, \\ h_{\text{merger}}(t), & T_{\text{ISCO}} < t < T_{\text{QNR}}, \\ h_{\text{ringdown}}(t), & T_{\text{QNR}} < t < \infty, \end{cases} \tag{18}$$

where T_{ISCO} is the time when the system reaches the ISCO and T_{QNR} is the time when the quasi-normal mode $l = m = 2$ begins to dominate the ringdown, although there is some arbitrariness in choosing T_{ISCO} and T_{QNR} to delimit the three epochs.

4.1. The inspiral waveform

For a non-spinning compact binary system with circular orbits, the two polarizations h_+ and $h_\times$ of the inspiral waveform can be well described by the post-Newtonian expansion. Thus, setting $G = c = 1$, they read

$$h_{+,\times} = \frac{2M\eta}{r}(M\omega)^{2/3}\left\{H^{(0)}_{+,\times} + v^{1/2}H^{(1/2)}_{+,\times} + vH^{(1)}_{+,\times} + v^{3/2}H^{(3/2)}_{+,\times} + v^2H^{(2)}_{+,\times} + \cdots\right\}, \tag{19}$$

where $v \equiv (M\omega)^{2/3}$, ω is the orbital frequency, r is the distance to the source, $M = m_1 + m_2$ is the total mass, $\mu = m_1m_2/M$ is the reduced mass, $\eta = \mu/M$ is the symmetric mass ratio and $\mathcal{M} = \mu^{3/5}M^{2/5} = M\eta^{3/5}$ is the chirp mass.

In what follows, we consider the waveform in the restricted post-Newtonian approximation [43], corresponding to a frequency twice the orbital frequency, and we ignore higher order harmonics. This corresponds to the lowest terms in the series (19). The functions $H^{(0)}_+$, $H^{(0)}_\times$ are given by [10]

$$H^{(0)}_+ = -(1 + \cos\iota^2)\cos\Phi(t), \tag{20}$$

$$H^{(0)}_\times = -2\cos\iota\sin\Phi(t), \tag{21}$$

with ι being the angle between the orbital angular momentum of the binary and the line of sight from the detector to the source. Φ is the phase of the gravitational wave at the instant t, that we consider modelled through second post-Newtonian order, neglecting the higher order terms in this analysis, since they would not contribute significantly to the result.

The Fourier transform of the inspiral waveform can be computed using the stationary phase approximation [33, 34, 39, 40] and this yields

$$\tilde{h}_{\rm INS}(f) = \begin{cases} \mathcal{A}_{\rm INS}f^{-7/6}\,\mathrm{e}^{\mathrm{i}\Psi(f)}, & f < f_{\rm ISCO}, \\ 0, & f > f_{\rm ISCO}, \end{cases} \tag{22}$$

with

$$\mathcal{A}_{\rm INS} = -\frac{\mathcal{M}^{5/6}}{r}\sqrt{\frac{5\pi}{96}}\pi^{-7/6}\sqrt{F_+^2(1+c^2)^2 + F_\times^2 4c^2}, \tag{23}$$

$$\Psi(f) = 2\pi f t_{\rm c} - \phi_{\rm c} - \frac{\pi}{4} + \frac{3}{128}\sum_{k=0}^{4}A_k u^{k-5}, \tag{24}$$

where $c = \cos\iota$, $t_{\rm c}$ refers to the coalescence time, $\phi_{\rm c}$ is the phase at the coalescence instant, $u = (\pi\mathcal{M}f)^{1/3}$ and the coefficients A_k are given by

$$A_0 = 1, \tag{25}$$

$$A_1 = 0, \tag{26}$$

$$A_2 = \tfrac{20}{9}\left(\tfrac{743}{336} + \tfrac{11}{4}\eta\right)\eta^{-2/5}, \tag{27}$$

$$A_3 = -16\pi\eta^{-3/5}, \tag{28}$$

$$A_4 = 10\left(\tfrac{3058\,673}{1016\,064} + \tfrac{5429}{1008}\eta + \tfrac{617}{144}\eta^2\right)\eta^{-4/5}. \tag{29}$$

We also consider the ISCO to take place at a separation of $6M$, corresponding to a final frequency

$$f_{\rm ISCO} = \frac{1}{6^{3/2}\pi M}. \tag{30}$$

4.2. The ringdown waveform

The ringdown portion of the gravitational wave signal we consider can be described as the $l = m = 2$ quasi-normal mode. Therefore, the gravitational radiation in the time domain is expected as the superposition of two different damped sinusoids, although one of these exponentials could be invisible in the actual waveform as discussed in [38]. In our study, we assume that the ringdown waveform can be written as in [25], corresponding to a circularly polarized wave. In this way, we have

$$h_+(t) - \mathrm{i}h_\times(t) = \frac{AM}{r}\,{}_2S_2^2(\iota, \beta, a)\exp\left[-\mathrm{i}2\pi f_{\mathrm{QNR}}(t - t_0) - \frac{\pi f_{\mathrm{QNR}}}{Q}(t - t_0) + \mathrm{i}\varphi_0\right], \tag{31}$$

where t_0 is the start time of the ringdown, φ_0 is the initial phase, M is the total mass of the system mass (see [45] for further discussions), and f_{QNR} and Q are the central frequency and the quality factor of the ringing, respectively. For this mode, a good fit to the frequency f_{QNR} and quality factor Q, within an accuracy of 5%, is

$$f_{\mathrm{QNR}} \approx [1 - 0.63(1 - a)^{3/10}]\frac{1}{2\pi M}, \tag{32}$$

$$Q \approx 2(1 - a)^{-9/20}, \tag{33}$$

where aM^2 is its spin and a is the Kerr parameter that lies in the range $(0.0, 0.998)$. In our study, we set a to the near-extremal value of 0.98 (as in [26]), although we consider a as any other independent parameter when evaluating the Fisher matrix. The function ${}_2S_2^2$ is the spin-weighted spheroidal harmonic that depends on the inclination angle of the black-hole axis seen from the observer and the Kerr parameter a. A is a dimensionless coefficient describing the magnitude of the perturbation when the ringdown begins. Although the value of the amplitude is uncertain, we set the amplitude of this mode by assuming that a fraction ϵ of the system's mass is converted into gravitational waves during the ringdown [26]

$$E_{\mathrm{RD}} \approx \frac{1}{8}A^2M^2 f_{\mathrm{QNR}}Q = \epsilon M\left(\frac{4\mu}{M}\right)^2. \tag{34}$$

Therefore,

$$A = \sqrt{\frac{128\eta^2\epsilon}{Mf_{\mathrm{QNR}}Q}}. \tag{35}$$

The strain produced at the detector can be written as

$$h_{\mathrm{RD}}(t) = \mathcal{A}_{\mathrm{RD}}\exp\left[-\frac{(t - t_0)\pi f_{\mathrm{QNR}}}{Q}\right]\cos(-2\pi f_{\mathrm{QNR}}(t - t_0) + \gamma_0), \tag{36}$$

where

$$\mathcal{A}_{\mathrm{RD}} \equiv \frac{AM}{r}\sqrt{F_+^2 + F_\times^2}\,|{}_2S_2^2|. \tag{37}$$

The Fourier transform of the waveform becomes

$$\tilde{h}_{\mathrm{RD}}(f) = \frac{\mathcal{A}_{\mathrm{RD}}}{2\pi}\,\mathrm{e}^{\mathrm{i}2\pi f t_0}\left(\frac{\mathrm{e}^{\mathrm{i}\gamma_0}}{\frac{f_{\mathrm{QNR}}}{Q} - 2\mathrm{i}(f - f_{\mathrm{QNR}})} + \frac{\mathrm{e}^{-\mathrm{i}\gamma_0}}{\frac{f_{\mathrm{QNR}}}{Q} - 2\mathrm{i}(f + f_{\mathrm{QNR}})}\right). \tag{38}$$

5. Parameter estimation of compact binaries using the inspiral and ringdown waveforms

In this paper, we want to study the impact on the parameter extraction by combining the signals from the inspiral and the ringdown epochs, neglecting all information coming from the merger epoch itself since no reliable waveforms exist so far.

Following earlier works, we choose the set of independent parameter $\lambda_{\rm INS}$ describing the inspiral signal to be

$$\lambda_{\rm INS} = \{\ln \mathcal{A}_{\rm INS},\, f_0 t_{\rm c},\, \phi_{\rm c},\, \ln \mathcal{M},\, \ln \eta\}, \tag{39}$$

while for the ringdown the parameters could be

$$\lambda_{\rm RD} = \{\ln \mathcal{A}_{\rm RD},\, \ln M,\, \ln a,\, \gamma_0,\, t_0\}. \tag{40}$$

A possible approach to this problem of parameter extraction would be to consider the two sets of parameters (39) and (40) as independent, perform matched filtering using the two template families (for the inspiral and the ringdown waveforms) and then reduce the uncertainties in the parameter estimation (in particular for the masses) by making a posterior consistency check [46]. However, in this paper we follow a different approach. We consider only a single coalescing waveform, as if we were performing matched filtering with a single template family bank, as given by equation (18), which describes the different phases, but ignoring the information from the merger phase, and we focus our attention on how parameter estimation of the $\lambda_{\rm INS}$ parameters can be improved as compared to the case in which the inspiral waveform is used alone. For this reason, the study presented here focuses only on those mass ranges for which the inspiral signal alone could be detectable by the detector. This corresponds to a total mass of approximately 1–100 $M_\odot$ for initial LIGO, 1–400 $M_\odot$ for advanced LIGO and 1–200 $M_\odot$ for VIRGO.

The global waveform considered here becomes in the Fourier domain

$$\tilde{h}_{\rm GL}(f) = \tilde{h}_{\rm INS}(f) + \tilde{h}_{\rm RD}(f), \tag{41}$$

where $\tilde{h}_{\rm INS}(f)$ and $\tilde{h}_{\rm RD}(f)$ are given by equations (22) and (38), respectively. This global waveform is completely determined by a set of independent parameters, given by

$$\lambda_{\rm GL} = \{\ln \mathcal{A}_{\rm INS},\, f_0 t_{\rm c},\, \phi_{\rm c},\, \ln \mathcal{M},\, \ln \eta,\, \ln a,\, \gamma_0,\, t_0\}. \tag{42}$$

Note that we do not include $\ln \mathcal{A}_{\rm RD}$ as an independent parameter since for a given source location and orientation, and a given ringdown efficiency ϵ, the ringdown amplitude $\mathcal{A}_{\rm RD}$, given by equation (37), is determined by the inspiral amplitude $\mathcal{A}_{\rm INS}$, the Kerr parameter and the masses. Instead, what we do is to find a heuristic relation between $\mathcal{A}_{\rm RD}$ and $\mathcal{A}_{\rm INS}$ by averaging over source directions and black-hole orientations, making use of the angle averages: $\langle F_+^2 \rangle_{\theta,\phi,\psi} = \langle F_\times^2 \rangle_{\theta,\phi,\psi} = 1/5$, $\langle F_+ F_\times \rangle_{\theta,\phi,\psi} = 0$, $\langle c^2 \rangle_\iota = 1/3$, $\langle (1+c^2)^2 \rangle_\iota = 28/15$ and $\langle |{}_2S_2^2|^2 \rangle_{\iota,\beta} = 1/4\pi$. The angle-averaged root-mean-square (rms) values of the inspiral and ringdown amplitudes $\mathcal{A}_{\rm INS}$, $\mathcal{A}_{\rm RD}$, given by equations (23) and (37), become

$$\mathcal{A}_{\rm INS}^{\rm rms} \equiv \sqrt{\langle \mathcal{A}_{\rm INS}^2 \rangle} = \frac{1}{\sqrt{30}\pi^{2/3}} \frac{\mathcal{M}^{5/6}}{r}, \tag{43}$$

$$\mathcal{A}_{\rm RD}^{\rm rms} \equiv \sqrt{\langle \mathcal{A}_{\rm RD}^2 \rangle} = \frac{1}{\sqrt{10\pi}} \frac{AM}{r}. \tag{44}$$

From the above equations, together with equation (35), we derive a relation $\mathcal{A}_{\rm RD} = \mathcal{A}_{\rm RD}(\mathcal{A}_{\rm INS}, \mathcal{M}, \eta, a)$ through the ratio of rms of both amplitudes:

$$\mathcal{A}_{\rm RD}(\mathcal{A}_{\rm INS}, \mathcal{M}, \eta, a) \equiv \frac{\mathcal{A}_{\rm RD}^{\rm rms}}{\mathcal{A}_{\rm INS}^{\rm rms}} \mathcal{A}_{\rm INS} = \sqrt{\frac{384\pi^{1/3}\epsilon}{M f_{\rm QNR} Q}} \eta^{2/5} \mathcal{M}^{1/6} \mathcal{A}_{\rm INS}. \tag{45}$$

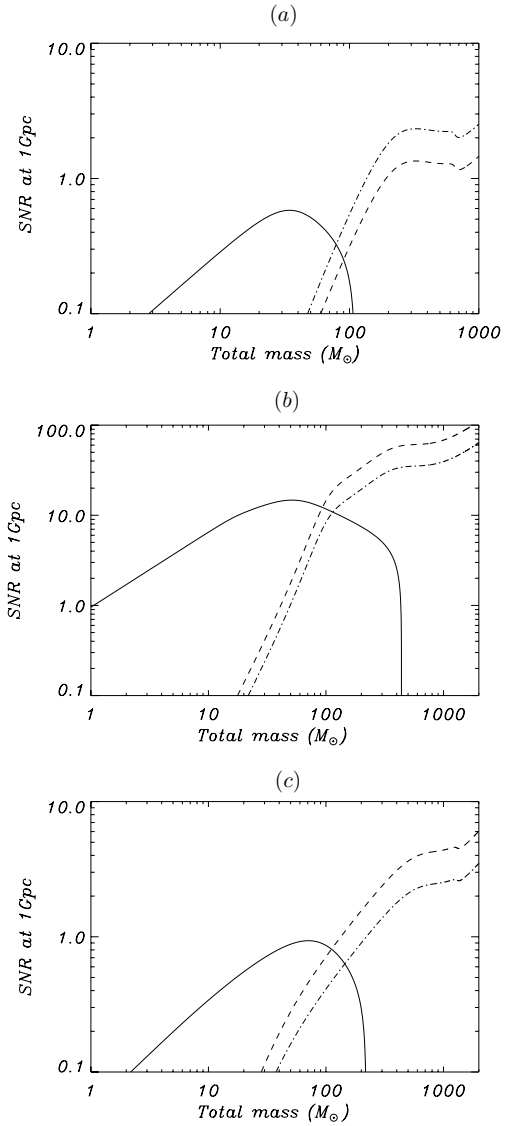

Figure 1. The averaged signal-to-noise ratio for equal-mass black-hole coalescences detected by ground-based interferometers at a luminosity distance of 1 Gpc. The solid line is the SNR curve for the inspiral, and the dashed and dash-dotted lines for the ringdown portion of the signal assuming a value of $a = 0.98$ and ϵ equal to 1.5% and 0.5%, respectively. (a) Corresponds to initial LIGO, (b) to advanced LIGO and (c) to VIRGO.

Note that in this relation the product of M and $f_{\rm QNR}$ is just a function of a as can be seen from equation (32). This relation (45) will be used in calculating the SNR as well as the Fisher matrix for the global waveform.

The SNR values for equal-mass black-hole binaries are shown in figure 1. This figure indicates that there is a range of masses (different for the different noise curves) for which both the inspiral and the ringdown signals could be detectable and one could search for

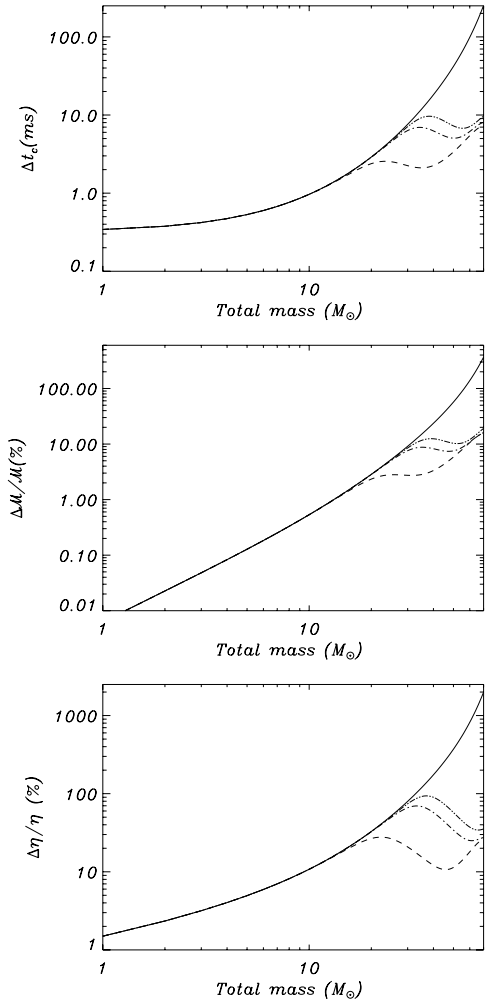

Figure 2. A comparison of errors in the estimation of t_c, $\mathcal{M}$ and η for equal-mass black-hole coalescences by the initial LIGO interferometers at a fixed inspiral SNR of 10. The solid line corresponds to the inspiral signal only and the others to the combined inspiral plus ringdown waveforms. The dashed line corresponds to the case in which only the five independent inspiral parameters (39) are considered for $\epsilon = 1.5\%$, while the dot-dashed lines correspond to the cases in which we consider all the independent global parameters (42) and ϵ equal to 1.5% and 0.5%, respectively.

both portions of the signal in order to improve the SNR and the accuracy in parameter estimation[3].

It is clear that both in the time domain and in the frequency domain, the inspiral signal is decoupled from the ringdown one. The inspiral waveform $\tilde{h}_{\rm INS}(f)$ ranges from the lower cut-off frequency f_s to $f_{\rm ISCO}$, while the ringdown $\tilde{h}_{\rm RD}(f)$ is centred around $f_{\rm QNR}$ with a certain

[3] The calculation of the SNR for the ringdown waveform is computed differently from what was done by Flanagan and Hughes in [26]. Instead of taking $|t - t_0|$ in the damped exponential, integrating over t over $-\infty$ to $+\infty$ and dividing the result by $\sqrt{2}$ to compensate for the doubling, we assume that the waveform $h_{\rm RD}(t)$ vanishes for $t < t_0$ and integrate only over $t > t_0$.

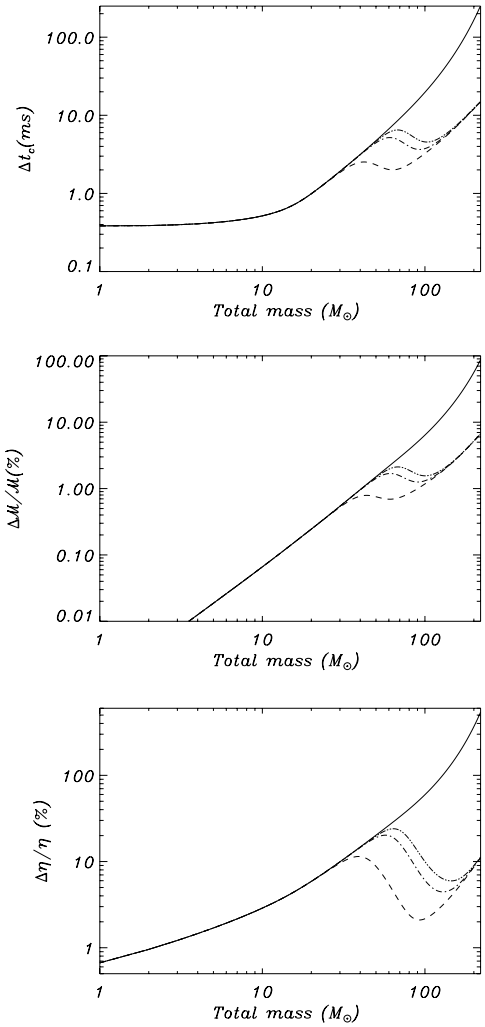

Figure 3. Same as figure 2 for advanced LIGO.

bandwidth, that in the literature is considered to be smaller than $\Delta f/f_{\rm QNR} = 0.5$,[4] although in our numerical simulations for the ringdown signal we use the same lower cut-off frequency $f_{\rm s}$ and a higher cut-off frequency of 5000 Hz. This justifies that the Fisher matrix, defined in equation (11), of the global waveform can be computed as

$$\Gamma_{ij} = (\partial_i h_{\rm GL}|\partial_j h_{\rm GL}) = (\partial_i h_{\rm INS}|\partial_j h_{\rm INS}) + (\partial_i h_{\rm RD}|\partial_j h_{\rm RD}), \tag{46}$$

neglecting the cross elements $(\partial_i h_{\rm INS}|\partial_j h_{\rm RD})$. Therefore, the Fisher matrix can be computed as the sum of the Fisher matrix of the inspiral waveform plus the Fisher matrix of the ringdown

$$\Gamma_{\rm GL} = \Gamma_{\rm INS} + \Gamma_{\rm RD}, \tag{47}$$

[4] Note that the distance between $f_{\rm QNR}$ and $f_{\rm ISCO}$ is larger than the bandwidth of the ringdown signal $\tilde{h}_{\rm RD}(f)$. In particular, if we consider the value $a = 0.98$ then $(f_{\rm QNR} - f_{\rm ISCO})/f_{\rm QNR} = 0.833$, which suggests no overlap between the inspiral and the ringdown signal.

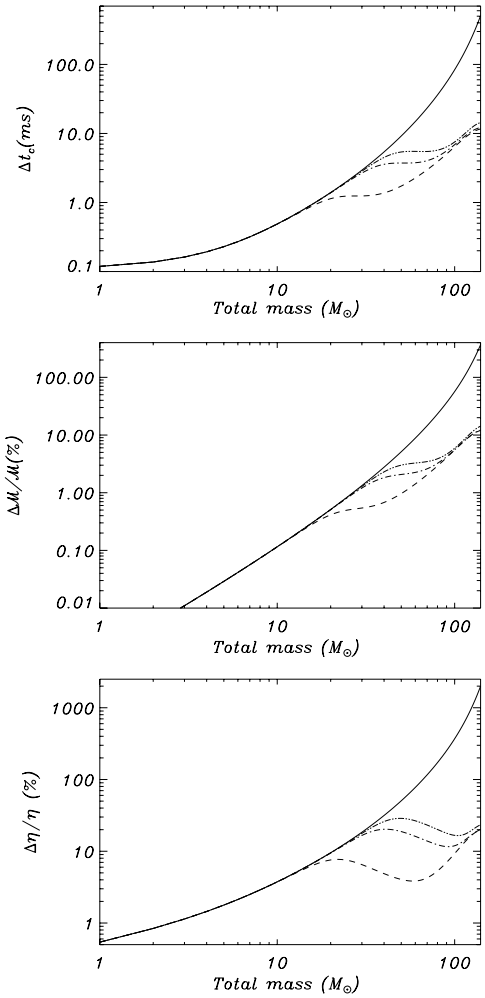

Figure 4. Same as figure 2 for VIRGO.

where we just need to be consistent in computing the elements corresponding to the same parameter set. Also, the total SNR is given by

$$\rho^2_{\mathrm{GL}} = \rho^2_{\mathrm{INS}} + \rho^2_{\mathrm{RD}}. \tag{48}$$

The way we proceed is to analyse first the well-known case of the inspiral signal alone, and then we compare the results with those when using the inspiral and ringdown waveforms together. In order to separate the effects of increasing the number of parameters from the fact that we are using a more complex waveform, we study two different cases.

(i) The case in which only the five inspiral parameters are considered. This is equivalent to having no uncertainties in the spin of the final black hole, nor in the initial phase and time of the ringdown signal. This, of course, would not be realistic in a search, but it provides the optimal improvement in parameter estimation one could expect from the fact that we added the ringdown waveform.

(ii) The more realistic case in which all eight independent parameters given in (42) are considered.

Table 1. Measurements of errors and some of the associated correlation coefficients using the second post-Newtonian binary inspiral waveform at a SNR of 10. For each of the three detector noise curves, the table presents Δt_c (in ms), $\Delta\phi_c$ (in rad), $\Delta\mathcal{M}/\mathcal{M}$ and $\Delta\eta/\eta$ (in percentage). The cases considered here correspond to NS–BH and BH–BH binaries of different masses.

m_1 ($M_\odot$)	m_2 ($M_\odot$)	Δt_c (ms)	$\Delta\phi_c$ (rad)	$\Delta\mathcal{M}/\mathcal{M}$ (%)	$\Delta\eta/\eta$ (%)	$C_{t_c\mathcal{M}}$	$C_{t_c\eta}$	$C_{\mathcal{M}\eta}$
Initial LIGO								
20	1.4	3.3708	7.8897	0.7873	10.6451	0.9294	0.9760	0.9847
50	1.4	47.2786	65.2176	6.5073	50.6737	0.9845	0.9953	0.9967
20	10	7.6032	15.0441	8.0579	72.3184	0.9573	0.9851	0.9918
60	10	253.505	291.931	176.566	1058.45	0.9947	0.9983	0.9990
Advanced LIGO								
25	1.4	1.5726	2.3121	0.0769	2.0304	0.8002	0.9397	0.9319
100	1.4	20.5373	11.5863	0.3354	3.9734	0.9426	0.9829	0.9859
200	1.4	171.714	59.9235	1.5215	12.2235	0.9836	0.9951	0.9965
100	10	24.9199	13.3081	2.5514	26.7760	0.9500	0.9843	0.9886
200	10	205.361	69.9572	12.1978	92.3077	0.9855	0.9955	0.9970
100	50	58.8914	25.7410	17.1443	133.132	0.9707	0.9901	0.9943
175	50	282.241	93.6166	66.6933	434.669	0.9884	0.9962	0.9978
VIRGO								
20	1.4	1.5875	2.8685	0.1339	3.0661	0.8619	0.9499	0.9679
100	1.4	89.3534	62.0062	3.1241	24.8609	0.9839	0.9951	0.9966
20	10	2.9432	4.3971	1.1712	16.7567	0.9025	0.9630	0.9805
50	10	14.9211	14.5300	4.7808	46.7855	0.9564	0.9853	0.9912
100	10	128.487	85.3035	28.3745	202.072	0.9874	0.9960	0.9975
70	50	198.798	128.504	135.517	804.327	0.9907	0.9968	0.9983
90	50	509.639	299.335	338.459	1865.97	0.9948	0.9982	0.9991

In appendix A, the reader can find the explicit calculations of all the waveform derivatives necessary to compute the Fisher matrix which is then computed numerically.

In our analysis, we set the Kerr parameter $a = 0.98$ (as in [26]), and we consider two different values of ϵ: a more optimistic value of 1.5% (half the value used in [26]) and a more pessimistic one of 0.5%, that are more consistent with recent numerical simulations [22]. With these parameters, we study a range of masses, analysing both the equal-mass and unequal-mass cases, for three ground-based detectors: initial LIGO, advanced LIGO and VIRGO, using the noise curves described in section 3. All the errors are computed at a fixed value of inspiral SNR of 10.

For the equal-mass case, the results are presented in figures 2–4 corresponding to initial LIGO, advanced LIGO and VIRGO, respectively. The errors of t_c, $\mathcal{M}$ and η and some of the associated correlation coefficients for the inspiral signal alone, for different pairs of masses, can be found in table 1. In tables 2 and 3, one can find the comparison of errors and correlation coefficients for the different cases we have analysed. In particular, table 2 refers to case (i) in which only the five inspiral parameters are considered and table 3 refers to case (ii) in which we use the eight global parameters. In all cases the errors improve, and the improvement is higher for larger masses for which the ringdown signal contribution to the SNR increases. This improvement could be explained not only by the greater structure and variety of the global waveform but also by the variation of some of the correlation coefficients, although this is not fully assessed in this paper. We have just noted that the correlation coefficients relative to the masses decrease when the ringdown signal is added, as can be seen in the tables. We also note that the improvement is very significant for massive systems with very large errors

Table 2. Measurements of errors and associated correlation coefficients using the second post-Newtonian binary inspiral waveform at a SNR of 10 together with the ringdown waveform, using a set of five parameters $\{\ln \mathcal{A}_{\rm INS},\, f_0 t_{\rm c},\, \phi_{\rm c},\, \ln \mathcal{M},\, \ln \eta\}$, excluding $\{\ln a,\, \gamma_0,\, t_0\}$.

ϵ (%)	m_1 ($M_\odot$)	m_2 ($M_\odot$)	$\frac{\Delta \mathcal{A}_{\rm INS}}{\mathcal{A}_{\rm INS}}$ (%)	$\Delta t_{\rm c}$ (ms)	$\Delta\phi_{\rm c}$ (rad)	$\Delta\mathcal{M}/\mathcal{M}$ (%)	$\Delta\eta/\eta$ (%)	$C_{t_{\rm c}\mathcal{M}}$	$C_{t_{\rm c}\eta}$	$C_{\mathcal{M}\eta}$	$\rho_{\rm GL}$
Initial LIGO											
1.5	20	1.4	9.9990	3.3424	7.8207	0.7807	10.5517	0.9282	0.9756	0.9844	10.0010
1.5	50	1.4	9.9697	14.8477	19.9568	2.0873	15.5191	0.8468	0.9513	0.9680	10.0304
1.5	20	10	9.9852	2.5040	4.5312	2.6880	21.6438	0.6113	0.8537	0.9239	10.0148
1.5	60	10	9.2208	9.7683	1.7464	10.3674	17.5337	−0.9594	−0.9369	0.9922	10.9880
0.5	20	1.4	9.9997	3.3613	7.8665	0.7851	10.6137	0.9290	0.9759	0.9846	10.0003
0.5	50	1.4	9.9899	23.1830	31.6986	3.2146	24.6364	0.9362	0.9803	0.9866	10.0101
0.5	20	10	9.9951	3.7473	7.1810	3.9909	34.4457	0.8250	0.9372	0.9660	10.0050
0.5	60	10	9.6889	10.2048	2.1410	10.8297	18.7519	−0.9490	−0.8894	0.9796	10.3398
Advanced LIGO											
1.5	25	1.4	9.9994	1.5723	2.3116	0.0769	2.0300	0.8002	0.9396	0.9318	10.0006
1.5	100	1.4	9.5820	14.3057	7.9691	0.2351	2.7291	0.8825	0.9644	0.9711	10.4363
1.5	200	1.4	7.9748	27.1408	8.3128	0.2626	1.7010	0.4037	0.7836	0.8779	12.5470
1.5	100	10	7.4090	3.9747	0.9300	0.4705	1.4721	−0.6895	−0.1562	0.7144	13.5008
1.5	200	10	4.4008	15.1787	1.2639	1.2077	2.1026	−0.9234	−0.8621	0.9726	23.1557
1.5	100	50	3.9049	6.6557	0.8229	2.2776	3.8235	−0.8769	−0.8672	0.9951	28.3348
1.5	175	50	4.7381	16.8821	1.1369	5.3223	8.8739	−0.9333	−0.9325	0.9997	47.1507
0.5	25	1.4	9.9998	1.5725	2.3119	0.0769	2.0302	0.8002	0.9397	0.9319	10.0002
0.5	100	1.4	9.8546	17.6073	9.8910	0.2882	3.3904	0.9221	0.9766	0.9809	10.1475
0.5	200	1.4	9.1638	42.2225	14.0443	0.3882	2.8678	0.7397	0.9155	0.9452	10.9152
0.5	100	10	8.8592	4.2986	1.2823	0.4993	2.3083	−0.4740	0.2010	0.6867	11.2882
0.5	200	10	6.4175	15.3235	1.4330	1.2144	2.2822	−0.8994	−0.7383	0.9295	15.6651
0.5	100	50	5.6355	6.6795	0.8354	2.2862	3.8925	−0.8744	−0.8461	0.9858	18.2835
0.5	175	50	5.2676	17.0019	1.1474	5.3641	8.9507	−0.9338	−0.9315	0.9991	28.4206
VIRGO											
1.5	20	1.4	9.9884	1.5739	2.8419	0.1328	3.0372	0.8595	0.9490	0.9673	10.0116
1.5	100	1.4	9.8123	23.6168	15.7433	0.8518	6.3184	0.7771	0.9281	0.9533	10.1916
1.5	20	10	9.8860	1.3595	1.8045	0.5264	6.7294	0.5307	0.8124	0.8998	10.1154
1.5	50	10	9.5906	2.5435	1.4330	0.8642	4.2425	−0.4119	0.2591	0.7145	10.4273
1.5	100	10	8.7416	8.8760	1.5912	2.6407	4.9586	−0.8994	−0.7351	0.9318	11.4628
1.5	70	50	8.0221	10.4639	1.1242	9.8663	16.4643	−0.9298	−0.9263	0.9987	15.1284
1.5	90	50	8.8177	12.3529	1.0874	11.8368	19.7325	−0.9136	−0.9119	0.9994	18.3197
0.5	20	1.4	9.9961	1.5830	2.8595	0.1335	3.0564	0.8611	0.9496	0.9677	10.0039
0.5	100	1.4	9.9362	37.4447	25.6283	1.3239	10.2789	0.9094	0.9719	0.9808	10.0643
0.5	20	10	9.9616	1.8724	2.6772	0.7371	10.1277	0.7565	0.9058	0.9501	10.0386
0.5	50	10	9.8577	3.1084	2.2677	1.0361	7.0748	0.0358	0.5871	0.7987	10.1444
0.5	100	10	9.5177	9.1524	2.1289	2.6903	5.9890	−0.8220	−0.4653	0.8587	10.5102
0.5	70	50	8.7160	10.3890	1.2208	9.7697	16.3850	−0.9375	−0.9251	0.9955	11.9564
0.5	90	50	9.0164	14.0215	1.1789	13.7140	22.8751	−0.9326	−0.9288	0.9987	13.3618

for the inspiral waveform alone. These large errors are associated with the small number of useful cycles of the inspiral signal of these systems [32]. Therefore, the effect induced in parameter estimation due to the inclusion of the ringdown signal could be understood in terms of additional number of gravitational wave cycles accumulated. Although, from the present analysis, it is not clear which of these considerations is the dominant aspect to completely understand the variation in parameter estimation observed with the global waveform.

The numerical results for the inspiral and the ringdown waveforms separately have been verified by comparing with those existing in the literature (for different masses and noise curves). Moreover, for the ringdown case alone we have also found good agreement with an analytical approximation as described in appendix B.

6. Conclusions

We have carried out a study to understand the implications of adding the ringdown to the inspiral signal on parameter estimation of non-spinning binaries using the covariance matrix.

Table 3. Measurements of errors and associated correlation coefficients using the second post-Newtonian binary inspiral waveform at a SNR of 10 together with the ringdown waveform, using a set of eight parameters $\{\ln \mathcal{A}_{\rm INS},\, f_0 t_{\rm c}, \phi_{\rm c}, \ln \mathcal{M}, \ln \eta, \ln a, \gamma_0, t_0\}$.

ϵ (%)	m_1 ($M_\odot$)	m_2 ($M_\odot$)	$\frac{\Delta \mathcal{A}_{\rm INS}}{\mathcal{A}_{\rm INS}}$ (%)	$\Delta t_{\rm c}$ (ms)	$\Delta \phi_{\rm c}$ (rad)	$\Delta \mathcal{M}/\mathcal{M}$ (%)	$\Delta \eta/\eta$ (%)	$C_{t_{\rm c}\mathcal{M}}$	$C_{t_{\rm c}\eta}$	$C_{\mathcal{M}\eta}$	$\rho_{\rm GL}$
Initial LIGO											
1.5	20	1.4	9.9991	3.3699	7.8874	0.7871	10.6420	0.9293	0.9760	0.9847	10.0010
1.5	50	1.4	9.9726	41.1566	56.7201	5.6682	44.0711	0.9796	0.9938	0.9957	10.0304
1.5	20	10	9.9867	6.5956	13.0066	6.9918	62.5063	0.9433	0.9801	0.9890	10.0148
1.5	60	10	9.3295	11.0001	4.9916	10.5193	22.7730	−0.7781	−0.3566	0.8522	10.9880
0.5	20	1.4	9.9997	3.3705	7.8889	0.7872	10.6441	0.9294	0.9760	0.9847	10.0003
0.5	50	1.4	9.9907	44.9413	61.9743	6.1869	48.1536	0.9829	0.9948	0.9964	10.0101
0.5	20	10	9.9955	7.2160	14.2620	7.6482	68.5521	0.9526	0.9834	0.9908	10.0050
0.5	60	10	9.7394	12.6647	8.1550	11.5177	32.7242	−0.5226	0.0717	0.8049	10.3398
Advanced LIGO											
1.5	25	1.4	9.9995	1.5726	2.3120	0.0769	2.0304	0.8002	0.9397	0.9319	10.0006
1.5	100	1.4	9.6291	20.2342	11.4112	0.3305	3.9132	0.9409	0.9824	0.9855	10.4363
1.5	200	1.4	8.1761	100.5296	34.8762	0.8944	7.1141	0.9524	0.9855	0.9898	12.5470
1.5	100	10	7.6653	7.6876	3.6663	0.8168	7.2850	0.4943	0.8220	0.8837	13.5008
1.5	200	10	4.7707	16.9594	2.8159	1.2761	3.8796	−0.6381	−0.0433	0.7703	23.1557
1.5	100	50	4.1663	6.7824	0.9771	2.2953	4.5952	−0.8306	−0.6018	0.8899	28.3348
1.5	175	50	4.8136	16.9720	1.2004	5.3227	8.9546	−0.9283	−0.9057	0.9909	47.1507
0.5	25	1.4	9.9998	1.5726	2.3121	0.0769	2.0304	0.8002	0.9397	0.9319	10.0002
0.5	100	1.4	9.8716	20.4346	11.5270	0.3338	3.9530	0.9421	0.9827	0.9858	10.1475
0.5	200	1.4	9.2305	132.9684	46.3067	1.1798	9.4457	0.9727	0.9917	0.9942	10.9152
0.5	100	10	8.9967	11.4032	5.8388	1.1846	11.6961	0.7646	0.9230	0.9461	11.2882
0.5	200	10	6.8066	19.8847	4.4807	1.4050	5.9807	−0.2786	0.3719	0.7714	15.6651
0.5	100	50	5.9767	7.0260	1.2240	2.3409	5.8647	−0.7460	−0.3025	0.7993	18.2835
0.5	175	50	5.4400	17.2493	1.3221	5.3654	9.1950	−0.9194	−0.8559	0.9743	28.4206
VIRGO											
1.5	20	1.4	9.9894	1.5871	2.8676	0.1339	3.0652	0.8619	0.9498	0.9679	10.0116
1.5	100	1.4	9.8253	71.2674	49.3691	2.4945	19.7938	0.9747	0.9923	0.9946	10.1916
1.5	20	10	9.8943	2.7362	4.0693	1.0874	15.4957	0.8870	0.9570	0.9774	10.1154
1.5	50	10	9.6406	6.5355	6.0863	2.1034	19.5048	0.7740	0.9210	0.9537	10.4273
1.5	100	10	8.9350	11.7992	5.2447	3.0553	12.5793	−0.2535	0.3875	0.7797	11.4628
1.5	70	50	8.0194	10.1883	1.6360	9.0353	15.5288	−0.9005	−0.7771	0.9528	15.1284
1.5	90	50	8.8495	12.9812	1.4506	11.9826	19.7503	−0.9062	−0.8606	0.9839	18.3197
0.5	20	1.4	9.9964	1.5874	2.8682	0.1339	3.0658	0.8619	0.9499	0.9679	10.0039
0.5	100	1.4	9.9386	81.8448	56.7624	2.8626	22.7583	0.9808	0.9942	0.9959	10.0643
0.5	20	10	9.9641	2.8685	4.2790	1.1410	16.3023	0.8973	0.9610	0.9795	10.0386
0.5	50	10	9.8721	9.4181	9.0312	3.0223	29.0276	0.8908	0.9627	0.9778	10.1444
0.5	100	10	9.6003	15.8131	8.7251	3.8272	20.7374	0.2455	0.7029	0.8553	10.5102
0.5	70	50	8.8855	11.2685	2.2537	9.7760	18.2478	−0.8595	−0.5971	0.9003	11.9564
0.5	90	50	9.0797	15.2788	1.9791	13.9267	22.9881	−0.9111	−0.8146	0.9655	13.3618

We have compared the results using three different noise curves corresponding to initial LIGO, advanced LIGO and VIRGO.

The result of our study is that the parameter estimation of $t_{\rm c}$, $\phi_{\rm c}$, $\mathcal{M}$ and η improves significantly, as expected, by employing the extra information that comes from the ringdown, for those systems with a total mass such that both the inspiral and the ringdown signal could be detectable by the detectors. Naturally, the improvement is larger in the case of considering a smaller number of parameters, but in both cases, the five-parameter case and the eight-parameter case, the improvement is significant. The study is performed at a fixed inspiral SNR of 10; therefore, the error in $\Delta \mathcal{A}_{\rm INS}/\mathcal{A}_{\rm INS}$ would be 10% for the inspiral signal alone. This is also improved by adding the ringdown.

In this work, we have made a number of simplifying assumptions, ignoring the merger phase, considering only the second post-Newtonian inspiral phase formula instead of the 3.5 that is already known, using only a single mode for the ringdown signal and ignoring angular dependences (because of the angle averages we use). For this reason, the results obtained here should be considered just as an indication of what could be the real effect in the parameter estimation by combining the inspiral with the ringdown signal. The preliminary

results obtained here seem to be very encouraging. Therefore, it would be interesting to extend the analysis to a more realistic case and also for different data analysis techniques (different from matched filtering). Although we have focused on ground-based detectors, a similar study could be performed for LISA.

Acknowledgments

The authors gratefully acknowledge the support of the Spanish Ministerio de Educación y Ciencia research project FPA-2004-03666.

Appendix A. The waveform derivatives

In order to calculate the Fisher matrix with respect to the $\{\ln \mathcal{A}_{\rm INS}, f_0 t_{\rm c}, \phi_{\rm c}, \ln \mathcal{M}, \ln \eta, \ln a, \gamma_0, t_0\}$ basis, we need to first compute the waveform derivatives. For the inspiral waveform $\tilde{h}_{\rm INS}(f)$, these are the following:

$$\frac{\partial \tilde{h}_{\rm INS}}{\partial \ln \mathcal{A}_{\rm INS}} = \tilde{h}_{\rm INS}, \tag{A.1}$$

$$\frac{\partial \tilde{h}_{\rm INS}}{\partial f_0 t_{\rm c}} = {\rm i}2\pi (f/f_0)\tilde{h}_{\rm INS}, \tag{A.2}$$

$$\frac{\partial \tilde{h}_{\rm INS}}{\partial \phi_{\rm c}} = -{\rm i}\tilde{h}_{\rm INS}, \tag{A.3}$$

$$\frac{\partial \tilde{h}_{\rm INS}}{\partial \ln \mathcal{M}} = {\rm i}\frac{1}{128}\sum_{k=0}^{4} A_k (k-5) u^{k-5} \tilde{h}_{\rm INS}, \tag{A.4}$$

$$\frac{\partial \tilde{h}_{\rm INS}}{\partial \ln \eta} = {\rm i}\frac{3}{128}\sum_{k=0}^{4} B_k u^{k-5} \tilde{h}_{\rm INS}, \tag{A.5}$$

where the parameters A_k are given by equations (25)–(29) and B_k are

$$B_0 = \frac{\partial A_0}{\partial \ln \eta} = 0, \tag{A.6}$$

$$B_1 = \frac{\partial A_1}{\partial \ln \eta} = 0, \tag{A.7}$$

$$B_2 = \frac{\partial A_2}{\partial \ln \eta} = \left(-\frac{743}{378} + \frac{11}{3}\eta\right)\eta^{-2/5}, \tag{A.8}$$

$$B_3 = \frac{\partial A_3}{\partial \ln \eta} = \frac{48}{5}\pi \eta^{-3/5}, \tag{A.9}$$

$$B_4 = \frac{\partial A_4}{\partial \ln \eta} = \left(-\frac{3058\,673}{127\,008} + \frac{5429}{504}\eta + \frac{617}{12}\eta^2\right)\eta^{-4/5}. \tag{A.10}$$

The inspiral waveform has no dependence on $\ln a$, γ_0 and t_0. Therefore, the remaining derivatives vanish

$$\frac{\partial \tilde{h}_{\rm INS}}{\partial \ln a} = \frac{\partial \tilde{h}_{\rm INS}}{\partial \gamma_0} = \frac{\partial \tilde{h}_{\rm INS}}{\partial t_0} = 0. \tag{A.11}$$

The derivatives of the ringdown waveform $\tilde{h}_{\rm RD}(f)$ can be computed by taking into account the implicit dependences of $\mathcal{A}_{\rm RD}(\mathcal{A}_{\rm INS}, \mathcal{M}, \eta, a)$, $f_{\rm QNR}(\mathcal{M}, \eta, a)$ and $Q(a)$. We get

$$\frac{\partial \tilde{h}_{\rm RD}}{\partial \ln \mathcal{A}_{\rm INS}} = \tilde{h}_{\rm RD}, \tag{A.12}$$

$$\frac{\partial \tilde{h}_{\rm RD}}{\partial \ln \mathcal{M}} = \frac{1}{6}\tilde{h}_{\rm RD} - \frac{\partial \tilde{h}_{\rm RD}}{\partial \ln f_{\rm QNR}}, \tag{A.13}$$

$$\frac{\partial \tilde{h}_{\rm RD}}{\partial \ln \eta} = \frac{2}{5}\tilde{h}_{\rm RD} + \frac{3}{5}\frac{\partial \tilde{h}_{\rm RD}}{\partial \ln f_{\rm QNR}}, \tag{A.14}$$

$$\begin{aligned}\frac{\partial \tilde{h}_{\rm RD}}{\partial \ln a} = {} & \frac{9(-100 + 21(1-a)^{3/10}a)}{40(-100 + 63(1-a)^{3/10})(-1+a)}\tilde{h}_{\rm RD} \\ & + \frac{189a}{10(-63 + 100(1-a)^{7/10} + 63a)}\frac{\partial \tilde{h}_{\rm RD}}{\partial \ln f_{\rm QNR}} + \frac{9a}{20(1-a)}\frac{\partial \tilde{h}_{\rm RD}}{\partial \ln Q},\end{aligned} \tag{A.15}$$

where

$$\frac{\partial \tilde{h}_{\rm RD}}{\partial \ln f_{\rm QNR}} = \frac{\mathcal{A}_{\rm RD}\, e^{2i f \pi t_0} f_{\rm QNR}}{2\pi}\left(\frac{e^{i\gamma_0}(2iQ+1)Q}{(f_{\rm QNR}(i-2Q)+2fQ)^2} + \frac{e^{-i\gamma_0}(1-2iQ)Q}{(2fQ + f_{\rm QNR}(2Q+i))^2}\right), \tag{A.16}$$

$$\frac{\partial \tilde{h}_{\rm RD}}{\partial \ln Q} = \frac{\mathcal{A}_{\rm RD}\, e^{2i f \pi t_0} f_{\rm QNR}}{2\pi Q}\left(\frac{e^{i\gamma_0}}{\left(f_{\rm QNR}\left(2i + \frac{1}{Q}\right) - 2if\right)^2} + \frac{e^{-i\gamma_0}}{\left(\frac{f_{\rm QNR}}{Q} - 2i(f + f_{\rm QNR})\right)^2}\right). \tag{A.17}$$

The remaining derivatives are

$$\frac{\partial \tilde{h}_{\rm RD}}{\partial \gamma_0} = \frac{\mathcal{A}_{\rm RD}\, e^{2i f \pi t_0}}{2\pi}\left(\frac{i\, e^{i\gamma_0}}{\frac{f_{\rm QNR}}{Q} - 2i(f - f_{\rm QNR})} - \frac{i\, e^{-i\gamma_0}}{\frac{f_{\rm QNR}}{Q} - 2i(f + f_{\rm QNR})}\right), \tag{A.18}$$

$$\frac{\partial \tilde{h}_{\rm RD}}{\partial t_0} = 2i f \pi \tilde{h}_{\rm RD}, \tag{A.19}$$

$$\frac{\partial \tilde{h}_{\rm RD}}{\partial f_0 t_{\rm c}} = \frac{\partial \tilde{h}_{\rm RD}}{\partial \phi_{\rm c}} = 0. \tag{A.20}$$

Appendix B. Analytical analysis of the Fisher matrix for the ringdown waveform

In what follows, we are interested in finding an analytical approximation to the Fisher matrix for the ringdown waveform in order to compare and verify the numerical results obtained with a Fortran code. For this comparison, let us focus on the simpler case with five parameters, in which we are interested in computing the Fisher matrix with respect to the basis $(\ln \mathcal{A}_{\rm INS}, f_0 t_{\rm c}, \phi_{\rm c}, \ln \mathcal{M}, \ln \eta)$, thus assuming that there are no uncertainties in the parameters $(\ln a, \gamma_0, t_0)$. Of course, the ringdown signal does not depend on $f_0 t_{\rm c}$ and $\phi_{\rm c}$;

therefore, the problem is reduced to three parameters, although the signal would depend only on two independent ones, e.g. $(\ln \mathcal{A}_{\rm RD}, \ln f_{\rm QNR})$.

The way we proceed is to compute first the Fisher matrix of the ringdown signal with respect to $(\ln \mathcal{A}_{\rm RD}, \ln f_{\rm QNR})$. Assuming constant noise over the bandwidth of the signal[5], and taking the δ-function approximation as in [35], the elements $\Gamma_{\ln \mathcal{A} \ln \mathcal{A}}$ and $\Gamma_{\ln f_{\rm QNR} \ln f_{\rm QNR}}$ can be computed analytically using Mathematica. For $\gamma_0 = 0$, we get[6]

$$\Gamma_{\ln \mathcal{A}_{\rm RD} \ln \mathcal{A}_{\rm RD}} = \frac{2\mathcal{A}_{\rm RD}^2 Q(1+2Q^2)}{\pi(1+4Q^2) f_{\rm QNR} S_n(f_{\rm QNR})} \tag{B.1}$$

and

$$\Gamma_{\ln f_{\rm QNR} \ln f_{\rm QNR}} = \frac{\mathcal{A}_{\rm RD}^2 Q(1+4Q^2+8Q^8)}{\pi(1+4Q^2) f_{\rm QNR} S_n(f_{\rm QNR})}. \tag{B.2}$$

For the cross term $\Gamma_{\ln \mathcal{A} \ln f_{\rm QNR}}$, Finn's approximation [35] can no longer be employed, because $\partial \tilde{h}_{\rm RD}/\partial \ln f_{\rm QNR}$ is not a symmetric function around $f_{\rm QNR}$. In order to compute this term, we will consider the following properties we have derived.

The reader should note that for any set of parameters $(\ln \mathcal{A}, \{\lambda^i\})$ and any waveform of the form

$$\tilde{h}(\mathcal{A}, \{\lambda^i\}, f) = \mathcal{A}\tilde{H}(\{\lambda^i\}, f), \tag{B.3}$$

the elements of the Fisher matrix satisfy the relations

$$\Gamma_{\ln \mathcal{A} \lambda^i} = \frac{1}{2} \frac{\partial \Gamma_{\ln \mathcal{A} \ln \mathcal{A}}}{\partial \lambda^i}, \tag{B.4}$$

$$\Gamma_{ij} = \partial_j \Gamma_{\ln \mathcal{A} \lambda^i} - (h|\partial_{ij} h). \tag{B.5}$$

Then using the standard definition of SNR given by equation (9) we have

$$\Gamma_{\ln \mathcal{A} \ln \mathcal{A}} = \rho^2, \tag{B.6}$$

and consequently

$$\Gamma_{\ln \mathcal{A} \lambda^i} = \tfrac{1}{2} \partial_i \rho^2. \tag{B.7}$$

These relations hold true for both the inspiral and the ringdown signals when considering $\mathcal{A}$ to be the amplitude of the signal. In the case of the ringdown signal, using equations (B.1), (B.6) and (B.7) we get

$$\rho_{\rm RD}^2 = \frac{2\mathcal{A}_{\rm RD}^2 Q(1+2Q^2)}{\pi(1+4Q^2) f_{\rm QNR} S_n(f_{\rm QNR})}, \tag{B.8}$$

$$\Gamma_{\ln \mathcal{A}_{\rm RD} \ln f_{\rm QNR}} = -\frac{1}{2} \rho_{\rm RD}^2 (1+S), \tag{B.9}$$

where

$$S = \frac{1}{S_n(f_{\rm QNR})} \frac{{\rm d}S_n(f_{\rm QNR})}{{\rm d} \ln f_{\rm QNR}}. \tag{B.10}$$

[5] The approximation that the noise is constant over the bandwidth of the signal is a good approximation for all the detectors considered here when $a \geqslant 0.9$ corresponding to $\Delta f/f_{\rm QNR} \leqslant 0.5$ as explained in [35]. In this paper, we consider only the case in which $a = 0.98$.

[6] If instead of using $\gamma_0 = 0$ we take $\gamma_0 = \pi/2$, then $\Gamma_{\ln \mathcal{A}_{\rm RD} \ln \mathcal{A}_{\rm RD}}$ becomes $4\mathcal{A}_{\rm RD}^2 Q^3/[\pi(1+4Q^2) f_{\rm QNR} S_n(f_{\rm QNR})]$ equivalent to Finn's result [35].

Table B1. Comparison of the analytical approximation and the numerical results, as described in the text, for the elements of the ringdown Fisher matrix for the initial LIGO detector assuming $a = 0.98$ and $\gamma_0 = 0$.

	Analytical	Numerical
$M = 20M_\odot$		
$\hat{\Gamma}_{\ln\mathcal{A}_{\rm INS}\ln\mathcal{M}}/\rho^2_{\rm RD}$	1.646	1.640
$\hat{\Gamma}_{\ln\mathcal{A}_{\rm INS}\ln\eta}/\rho^2_{\rm RD}$	−0.488	−0.484
$\hat{\Gamma}_{\ln\mathcal{M}\ln\mathcal{M}}/\rho^2_{\rm RD}$	288.52	276.33
$\hat{\Gamma}_{\ln\mathcal{M}\ln\eta}/\rho^2_{\rm RD}$	−172.29	−164.98
$\hat{\Gamma}_{\ln\eta\ln\eta}/\rho^2_{\rm RD}$	103.13	98.74
$M = 100M_\odot$		
$\hat{\Gamma}_{\ln\mathcal{A}_{\rm INS}\ln\mathcal{M}}/\rho^2_{\rm RD}$	1.299	1.276
$\hat{\Gamma}_{\ln\mathcal{A}_{\rm INS}\ln\eta}/\rho^2_{\rm RD}$	−0.279	−0.265
$\hat{\Gamma}_{\ln\mathcal{M}\ln\mathcal{M}}/\rho^2_{\rm RD}$	288.41	284.81
$\hat{\Gamma}_{\ln\mathcal{M}\ln\eta}/\rho^2_{\rm RD}$	−172.40	−170.25
$\hat{\Gamma}_{\ln\eta\ln\eta}/\rho^2_{\rm RD}$	103.30	102.02

Note that the δ-function approximation in this case is equivalent to considering $S = 0$, but this term is not negligible. For example, if we consider initial LIGO and a total mass of 10, 20 or 100 $M_\odot$, the corresponding S value would be 1.989, 1.959 and 1.264, respectively.

The Fisher matrix with respect to the basis $(\ln\mathcal{A}_{\rm INS}, \ln\mathcal{M}, \ln\eta)$ (which naturally will be degenerate) can easily be computed by taking into account the amplitude relation given by equation (45) and considering

$$\begin{pmatrix} \partial\tilde{h}_{\rm RD}/\partial\ln\mathcal{A}_{\rm INS} \\ \partial\tilde{h}_{\rm RD}/\partial\ln\mathcal{M} \\ \partial\tilde{h}_{\rm RD}/\partial\ln\eta \end{pmatrix} = \begin{pmatrix} 1 & 0 \\ 1/6 & -1 \\ 2/5 & 3/5 \end{pmatrix} \begin{pmatrix} \partial\tilde{h}_{\rm RD}/\partial\ln\mathcal{A}_{\rm RD} \\ \partial\tilde{h}_{\rm RD}/\partial\ln f_{\rm QNR} \end{pmatrix}. \tag{B.11}$$

If we define the constant matrix

$$\mathcal{C} \equiv \begin{pmatrix} 1 & 0 \\ 1/6 & -1 \\ 2/5 & 3/5 \end{pmatrix}, \tag{B.12}$$

let Γ be the Fisher matrix with respect to $(\ln\mathcal{A}_{\rm RD}, \ln f_{\rm QNR})$ and $\hat{\Gamma}$ the Fisher matrix with respect to $(\ln\mathcal{A}_{\rm INS}, \ln\mathcal{M}, \ln\eta)$, in this particular case, Γ and $\hat{\Gamma}$ are related in the following way:

$$\hat{\Gamma} = \mathcal{C}\Gamma\mathcal{C}^T, \tag{B.13}$$

where the superscript T indicates transposed matrix. The matrix $\hat{\Gamma}$ has the elements

$$\hat{\Gamma}_{\ln\mathcal{A}_{\rm INS}\ln\mathcal{A}_{\rm INS}} = \rho^2_{\rm RD}, \tag{B.14}$$

$$\hat{\Gamma}_{\ln\mathcal{A}_{\rm INS}\ln\mathcal{M}} = \rho^2_{\rm RD}\frac{4+3S}{6}, \tag{B.15}$$

$$\hat{\Gamma}_{\ln\mathcal{A}_{\rm INS}\ln\eta} = \rho^2_{\rm RD}\frac{1-3S}{10}, \tag{B.16}$$

$$\hat{\Gamma}_{\ln\mathcal{M}\ln\mathcal{M}} = \rho^2_{\rm RD}\frac{2(72Q^2+6S+43)Q^2+6S+25}{72Q^2+36}, \tag{B.17}$$

$$\hat{\Gamma}_{\ln\mathcal{M}\ln\eta} = \rho^2_{\rm RD}\frac{1}{60}\left(-72Q^2 + 9S - \frac{18}{2Q^2+1} + 13\right), \tag{B.18}$$

$$\hat{\Gamma}_{\ln\eta\ln\eta} = \rho^2_{\rm RD}\frac{1}{50}\left(36Q^2 - 12S + \frac{9}{2Q^2+1} - 4\right), \tag{B.19}$$

and trivially

$$\hat{\Gamma}_{f_0 t_c \lambda^i} = \hat{\Gamma}_{\phi_c \lambda^i} = 0. \tag{B.20}$$

The analytical approximation and the numerical results are compared in table B1 for the initial LIGO detector and two different values of the total mass.

References

[1] Willke B *et al* 2004 *Class. Quantum Grav.* **21** S417–23
[2] Grote H *et al* 2005 *Class. Quantum Grav.* **22** S193–8
[3] Abramovici A *et al* 1992 *Science* **256** 325
[4] Barish B and Weiss R 1999 *Phys. Today* **52** 44
[5] Tsubono K 1995 *1st Edoardo Amaldi Conf. Gravitational Wave Experiments* ed E Coccia, G Pizella and F Ronga (Singapore: World Scientific) p 112
[6] Caron B *et al* 1997 *Nucl. Phys.* B **54** 167
[7] Blanchet L 2002 Gravitational radiation from post-Newtonian sources and inspiralling compact binaries *Living Rev. Rel.* **5** 3 (http://www.livingreviews.org/lrr-2002-3, cited on 4 April 2006)
[8] Blanchet L 1995 *Phys. Rev.* D **51** 2559–83
[9] Blanchet L, Damour T, Iyer B R, Will C M and Wiseman A G 1995 *Phys. Rev. Lett.* **74** 3515–8
[10] Blanchet L, Iyer B R, Will C M and Wiseman A G 1996 *Class. Quantum Grav.* **13** 575–84
[11] Damour T, Iyer B R and Sathyaprakash B S 1998 *Phys. Rev.* D **57** 885–907
[12] Damour T, Jaranowski P and Schäfer G 2000 *Phys. Rev.* D **62** 021501
[13] Blanchet L, Damour T, Esposito-Farese G and Iyer B R 2004 *Phys. Rev. Lett.* **93** 091101
[14] Nissanke S and Blanchet L 2005 *Class. Quantum Grav.* **22** 1007–32
[15] Phinney E S 1991 *Astrophys. J.* **380** L17
[16] O'Shaughnessy R, Kalogera V and Belczynski K 2005 *Astrophys. J.* **620** 385–9
[17] O'Shaughnessy R, Kim C, Frakgos T, Kalogera V and Belczynski K 2005 *Astrophys. J.* **633** 1076–84
[18] Belczynski K, Kalogera V and Bulik T 2002 *Astrophys. J.* **572** 407–31
[19] Kalogera V, Narayan R, Spergel D N and Taylor J H 2001 *Astrophys. J.* **556** 340–56
[20] Bruegmann B, Tichy W and Jansen N 2004 *Phys. Rev. Lett.* **92** 211101
[21] Pretorius F 2005 *Phys. Rev. Lett.* **95** 121101
[22] Baker J, Brügmann B, Campanelli M, Lousto C O and Takahashi R 2001 *Phys. Rev. Lett.* **87** 121103
[23] Baker J, Campanelli M, Lousto C O and Takahashi R 2002 *Phys. Rev.* D **65** 124012
[24] Baker J, Campanelli M and Lousto C 2002 *Phys. Rev.* D **65** 044001
[25] Echevarria F 1988 *Phys. Rev.* D **40** 3194
[26] Flanagan E E and Hughes S A 1998 *Phys. Rev.* D **57** 4535
[27] Tsunesada Y, Kanda N, Nakano H, Tatsumi D, Ando M, Sasaki M, Tagoshi H and Takahashi H 2005 *Phys. Rev.* D **71** 103005
[28] Nakano H, Takahashi H, Tagoshi H and Sasaki M 2003 *Phys. Rev.* D **68** 102003
[29] Abbott B *et al* 2005 *Phys. Rev.* D **72** 082002
[30] Abbott B *et al* 2005 *Phys. Rev.* D **72** 082001
[31] Abbott B *et al* 2006 in preparation
[32] Arun K G, Iyer B R, Sathyaprakash B S and Sundararajan P A 2005 *Phys. Rev.* D **71** 084008
[33] Cutler C and Flanagan E E 1994 *Phys. Rev.* D **49** 2658
[34] Poisson E and Will C M 1995 *Phys. Rev.* D **52** 848–55
[35] Finn L S 1992 *Phys. Rev.* D **46** 5236–49
[36] Creighton J D E 1999 *Phys. Rev.* D **60** 022001
[37] Nakano H, Takahashi H, Tagoshi H and Sasaki M 2004 *Prog. Theor. Phys.* **111** 781–805
[38] Berti E, Cardoso V and Will C M 2006 *Phys. Rev.* D **73** 064030
[39] Sathyaprakash B S and Dhurandhar S V 1991 *Phys. Rev.* D **44** 3819
[40] Finn L S and Chernoff D F 1993 *Phys. Rev.* D **47** 2198

[41] Kokkotas K D and Schmidt B 1999 Quasi-normal modes of stars and black holes *Living Rev. Rel.* **2** 2 (http://www.livingreviews.org/lrr-1999-2, cited on 4 April 2006)
[42] Leaver E W 1985 *Proc. R. Soc. Lond.* A **402** 285
[43] Sintes A M and Vecchio A 2000 *Gravitational Waves and Experimental Gravity* ed J Tran Thanh Van, J Dumarchez, S Reynaud, C Salomon, S Thorsett and J Y Vinet (Hanoi, Vietnam: World Publishers) pp 73–8 (*Preprint* gr-qc/0005058)
[44] Thorne K S 1987 *300 Years of Gravitation* ed S W Hawking and W Israel (Cambridge: Cambridge University Press) p 330
[45] Hughes S A and Menou K 2005 *Astrophys. J.* **623** 689–99
[46] Sathyaprakash B S 2005 private communication